

Gauss-Bonnet Dark Energy and the Speed of Gravitational Waves

José Jaime Terente Díaz,¹ Konstantinos Dimopoulos,² Mindaugas Karčiauskas,¹ and Antonio Racioppi³

¹*Departamento de Física Teórica, Universidad Complutense de Madrid, E-28040 Madrid, Spain*

²*Consortium for Fundamental Physics, Physics Department, Lancaster University, Lancaster LA1 4YB, UK*

³*National Institute of Chemical Physics and Biophysics, Rävala 10, 10143 Tallinn, Estonia*

Gauss-Bonnet Dark Energy has been a popular model to explain the accelerated expansion of the Universe. Quite generically it also predicts the speed of gravitational waves c_{GW} to be different from the speed of light. This fact alone led some authors to exclude such models in view of the new tight observational constraints on c_{GW} . However, the behaviour of c_{GW} depends on the choice of the Gauss-Bonnet (GB) coupling function. It is possible to construct models where c_{GW} is always equal to the speed of light. More generally, c_{GW} is a time dependent function with instances where both speeds coincide. Nevertheless, we observe that the bound on c_{GW} excludes scenarios where the GB term directly affects the expansion of the Universe, even if the constraint on the variation of the coupling function does not appear to be strong. We perform the dynamical systems analysis to see if the expansion of the Universe could be affected indirectly by modulating the behaviour of the scalar field, which modulates the GB coupling. It is shown that either the bounds on c_{GW} are violated by many orders of magnitude, or it might be very difficult to find models that are consistent with other cosmological observations.

I. INTRODUCTION

The detection of gravitational waves (GW) [1–3] opens a new window to observe and measure the Universe. Most directly, it enables testing General Relativity (GR) in regimes that were not accessible before and constrain possible modifications of the laws of gravity. They also provide new ways to test Dark Energy (DE) models. Many of such models rely on gravity modifications and therefore are subject to such constraints.

A very clear demonstration is provided in Ref. [4]. A lucky coincidence of being able to detect GW emitted by the merger of two neutron stars as well as the electromagnetic counterpart of this event made it possible to put very stringent constraints on the speed of GW, c_{GW} . The delay between arrival times of GW and γ -rays led to the bound

$$|\alpha_T| < 10^{-15}, \quad (1)$$

where α_T parametrises the deviation of c_{GW} from the speed of light

$$\alpha_T \equiv c_{\text{GW}}^2 - 1, \quad (2)$$

in natural units, where $c = \hbar = 1$.

Many classes of modified gravity theories predict $\alpha_T \neq 0$. The constraints on α_T in Ref. [4] excluded a lot of well motivated and otherwise attractive models and considerably narrowed down the space of available modifications [5, 6].

Among the excluded models – it is claimed in Ref. [5] – is the Gauss-Bonnet Dark Energy (GBDE) one. This model has many attractive features. The Gauss-Bonnet term itself is a unique combination of curvature terms squared

$$\mathcal{G} \equiv R^2 - 4R_{\mu\nu}R^{\mu\nu} + R_{\mu\nu\rho\sigma}R^{\mu\nu\rho\sigma}, \quad (3)$$

where R , $R_{\mu\nu}$ and $R^{\rho}_{\sigma\mu\nu}$ are the Ricci scalar, tensor and Riemann tensor respectively. Nevertheless, this combination leads to metric tensor equations of motion that are second order. The Gauss-Bonnet (GB) term is quite ubiquitous in actions of low-energy effective string theory, be it at tree or one loop level [7–13]. The corresponding modification can be written as $\xi\mathcal{G}$ term in the Lagrangian, where ξ is the GB coupling. If the latter is a constant, the GB term is a surface term and can be integrated out (although it can still be important for other aspects of the theory, such as regularization [14, 15]). However, on quite generic grounds, one might expect that the GB term also couples to scalar fields of the theory, such as moduli or dilaton fields, making ξ field dependent.

The possibility of explaining DE with the GB term was first investigated in Refs. [16–20]. One of the attractive features of such models is that they provide the means to safely cross the phantom divide, that is, enter the regime where the DE equation of state is $w < -1$, without instabilities. The best fit value of w is smaller than -1 [21]. If such w is associated with a scalar field, it leads to many instabilities and such a model is likely excluded by observations [22]. On the other hand, modifications of gravity in GBDE in some parameter range allow for $w < -1$. In this model w is time dependent; it briefly dips below -1 before settling on $w = -1$ [18]. Hence, it can accommodate this low value without leading to contradictions.

Quite generically GBDE predicts $\alpha_T \neq 0$. This fact alone led the authors of Ref. [5] to claim that GBDE is ruled out. Here we would like to point out that c_{GW} , predicted by GBDE, is not a constant. Moreover, the constraint in eq. (1) is an upper bound which is applicable only at the very latest stages of the evolution of the Universe.¹ Hence, to assess the implications of these constraints for GBDE we need to study it more carefully.

In this work we use the dynamical systems analysis to look for viable models of GBDE and compute the evolution of α_T parameter. The crucial quantity in such models is the GB coupling $\xi(\phi)$. It determines the dynamics of the universe as well as the evolution of the α_T parameter. Applying the bound in eq. (1) to the variation of $\xi(\phi)$ and the rate of its variation, we find that the constraints appear weak. Nevertheless, the bound in eq. (1) prevents the GB term from affecting the expansion of the Universe directly. The remaining possibility is for this term to affect the expansion indirectly, by modifying the behaviour of the scalar field. To investigate this issue we apply the dynamical systems analysis. We also apply this analysis to the case where $\alpha_T = 0$ by construction, which is allowed by the model.

In Section II we introduce the model, derive dynamical equations and show the bounds on $\xi(\phi)$ that follow from eq. (1). In Section III we assume an exponential potential $V(\phi)$ and write the dynamical equations in terms of dimensionless variables, which are used in the following sections. The dynamical systems analysis is applied to models with the exponential GB coupling $\xi(\phi)$ in Section IV and it is applied to the linear function $\xi(\phi)$ in Section V. The case of $\alpha_T = 0$ is studied in Section VI.

II. SCALAR-GAUSS-BONNET DARK ENERGY AND CONSTRAINTS ON c_{GW}

We start with the scalar-Gauss-Bonnet action

$$S = \int d^4x \sqrt{-g} \left[\frac{1}{2} m_{\text{Pl}}^2 R + \xi(\phi) \mathcal{G} - \frac{1}{2} \partial_\mu \phi \partial^\mu \phi - V(\phi) + \mathcal{L}_m \right], \quad (4)$$

where \mathcal{G} is defined in eq. (3). For brevity we address to the above action as the Gauss-Bonnet (GB) action in this work. \mathcal{L}_m is the Lagrangian of the matter sector. If ξ is constant, the GB term is a total derivative and does not affect the dynamics of the system. We assume the background spacetime to be homogeneous, isotropic and flat, described by the FRW metric $g_{\mu\nu} = \text{diag}[-1, a^2(t), a^2(t), a^2(t)]$, where t is the cosmic time and a is the scale factor.

In this model the speed of tensor mode propagation is determined by the rate of change of the coupling function $\xi(\phi)$ [24–27] (see also Refs. [28, 29])

$$\alpha_T = \frac{8(\ddot{\xi} - \dot{\xi}H)}{m_{\text{Pl}}^2 + 8\dot{\xi}H}, \quad (5)$$

where we use a dot to denote the derivative with respect to t and $H \equiv \dot{a}/a$ is the Hubble parameter. It is clear from this expression that the constraint in eq. (1) can be satisfied if one of the following two conditions is fulfilled. The first option is to choose the coupling function $\xi(\phi)$ such that

$$\ddot{\xi} = H\dot{\xi}. \quad (6)$$

This choice is discussed in refs. [27, 30] (other related references can be found in these articles) in the context of inflation. However, there is another, more generic possibility. We notice in eq. (5) that α_T is suppressed by the Planck mass. Therefore, as long as the conditions $|\ddot{\xi}|/m_{\text{Pl}}^2, H|\dot{\xi}|/m_{\text{Pl}}^2 < 10^{-15}$ are satisfied, the GB action in eq. (4) is compatible with the constraints on the speed of gravitational waves. We can write these conditions in a more useful way

$$\frac{|\ddot{\xi}|}{H^2}, \frac{|\dot{\xi}|}{H} < 10^{-15} \left(\frac{m_{\text{Pl}}}{H} \right)^2, \quad (7)$$

which emphasises the change of the coupling function and the rate of change of this coupling over one Hubble time. If this condition is to be imposed on large field inflation models, where $H \lesssim 10^{-5} m_{\text{Pl}}$ [31], this bound can be tight. In that case, to limit α_T within the allowed range, it is better to look for models that satisfy the condition in eq. (6).

¹ It is also worth noting that the bound on α_T applies only to the limited range of GW frequencies. This fact alone could save many Horndeski type Dark Energy models [23].

However, the constraints from the observations of GRB170817A do not apply to the early Universe. Therefore it is not very useful to use them in that context. Instead, this constraint is applicable to the present Universe, within a very narrow range of e-folds (see Fig. 3), where the Hubble parameter is more than fifty orders of magnitude smaller than the value of H cited above. Indeed, plugging $H_0^2/m_{\text{Pl}}^2 \sim 10^{-120}$ [21] into eq. (7) we find²

$$\frac{|\ddot{\xi}|}{H_0^2}, \frac{|\dot{\xi}|}{H_0} < 10^{105}. \quad (8)$$

That is, ξ and $\dot{\xi}$ need to vary by more than 100 orders of magnitude, $\Delta\xi, \Delta\dot{\xi} < 10^{105}$, over the age of the Universe to violate the bound. This appears to demonstrate that the constraint on c_{GW} is exceptionally weak and might give hope that GBDE models remain viable. Unfortunately, as we show in this work, at least for simple functions $\xi(\phi)$, this turns out not to be the case.

To understand the implications of eq. (1) for Gauss-Bonnet Dark Energy (GBDE) models better, let us first write the homogeneous dynamical equations in the FRW background as [16, 32]

$$H^2 = \frac{\rho_\phi + \rho_m}{3(m_{\text{Pl}}^2 + 8H\dot{\xi})}, \quad (9)$$

$$\dot{H} = -\frac{\rho_\phi + P_\phi + \rho_m + P_m + 8H^2(\ddot{\xi} - \dot{\xi}H)}{2(m_{\text{Pl}}^2 + 8H\dot{\xi})}, \quad (10)$$

where ρ_ϕ and P_ϕ are the energy and pressure densities of the homogeneous scalar field ϕ respectively. They are defined to be

$$\rho_\phi \equiv \frac{1}{2}\dot{\phi}^2 + V(\phi), \quad (11)$$

$$P_\phi \equiv \frac{1}{2}\dot{\phi}^2 - V(\phi). \quad (12)$$

Similarly ρ_m and P_m are the energy and pressure densities of the matter field.

The acceleration of spatial slices can be parametrised using the Hubble flow parameter

$$\epsilon_H \equiv -\frac{\dot{H}}{H^2}. \quad (13)$$

Alternatively, it is common to use the deceleration parameter $q \equiv \epsilon_H - 1$ for this purpose. The spatial slices expand in an accelerating fashion if $\epsilon_H < 1$ ($q < 0$).

Plugging eqs. (9) and (10) into eq. (13) we can write

$$\epsilon_H = \frac{3}{2}\left(1 + \frac{P_\phi + P_m}{\rho_\phi + \rho_m}\right) + \frac{1}{2}\alpha_T, \quad (14)$$

where we also made use of eq. (5). At the present epoch $\epsilon_H \simeq 0.5$. Thus, in view of eq. (1) we see that the last term must be negligible. This rules out any direct effect of the Gauss-Bonnet term to the expansion of the Universe. Neglecting that last term, we arrive at the expression which can also be obtained in a typical, General Relativistic quintessence models [33, 34].

But even if observations exclude the scenario where the GB term affects the expansion of the Universe directly, there remains a possibility that it does so indirectly, by modifying the behaviour of the scalar field ϕ . As we will see next, such a possibility is also excluded, at least for an exponential potential $V(\phi)$.

III. THE DYNAMICAL SYSTEM

Equations (9) and (10) can be supplemented with dynamical equations governing the evolution of the ϕ field and ρ_m

$$\ddot{\phi} + 3H\dot{\phi} + V_{,\phi} = 24\xi_{,\phi}(\dot{H} + H^2)H^2, \quad (15)$$

$$\dot{\rho}_m + 3H\rho_m(1 + w_m) = 0, \quad (16)$$

² This is only an order of magnitude estimate. Factors of order 1 do not change the conclusions in any substantial way.

where $w_m \equiv P_m/\rho_m$ is the barotropic parameter of the matter component. And we assume a matter fluid with $0 \leq w_m < 1$.

To analyse the generic behaviour of this dynamical system, it is convenient to normalise the dynamical degrees of freedom and write them in a dimensionless form, such as

$$x \equiv \frac{\phi'}{\sqrt{6}m_{\text{Pl}}}, \quad y \equiv \frac{\sqrt{V}}{\sqrt{3}m_{\text{Pl}}H}, \quad u \equiv 4\sqrt{6}\frac{H^2\xi_{,\phi}}{m_{\text{Pl}}}, \text{ and } z \equiv \frac{\sqrt{\rho_m}}{\sqrt{3}m_{\text{Pl}}H}. \quad (17)$$

The prime in the definition of x and the equations below denotes the derivatives with respect to the e-fold number

$$N \equiv \ln a, \quad (18)$$

where we normalised a such that $a = 1$ today. The above defined dimensionless parameters are related to the more familiar density parameters by

$$\Omega_m \equiv \frac{\rho_m}{3m_{\text{Pl}}^2 H^2} = z^2, \quad (19)$$

$$\Omega_\phi \equiv \frac{\rho_\phi}{3m_{\text{Pl}}^2 H^2} = x^2 + y^2, \quad (20)$$

$$\Omega_{\text{GB}} \equiv -\frac{8H\dot{\xi}}{m_{\text{Pl}}^2} = -2ux. \quad (21)$$

The first two definitions are exactly the same as in models of GR with a scalar field. The physical origin of the last parameter is due to the modifications of gravity, but it is interpreted as an effective matter fluid. Following this interpretation we can write the constraint equation (9) (the Friedmann equation) as

$$1 = \Omega_\phi + \Omega_m + \Omega_{\text{GB}}. \quad (22)$$

In GR the analogous equation confines the range of variation of each parameter to $|\Omega| \leq 1$. This is due to the density parameters being non-negative. In GB gravity Ω_{GB} can be positive as well as negative. This makes it possible for Ω_ϕ and Ω_m to exceed unity.

The definitions in eq. (17) are particularly useful if the scalar field potential is an exponential function

$$V = V_0 e^{-\lambda\phi/m_{\text{Pl}}}, \quad (23)$$

where we take $\lambda > 0$ to be a constant. We will always use the above ansatz in this work. In that case the dynamical equations are self-similar and the explicit dependence on the Hubble parameter drops out of those equations. In particular, eqs. (15) and (16) can be written as

$$x' = (\epsilon_H - 3)x + \sqrt{\frac{3}{2}}\lambda y^2 + u(1 - \epsilon_H), \quad (24)$$

$$y' = \left(\epsilon_H - \sqrt{\frac{3}{2}}\lambda x\right)y, \quad (25)$$

$$z' = \left[\epsilon_H - \frac{3}{2}(1 + w_m)\right]z, \quad (26)$$

where

$$\epsilon_H = \left[3x^2 + \frac{3}{2}(1 + w_m)z^2 + (ux)' - ux\right]\frac{1}{1 + ux} \quad (27)$$

The constraint equation (22), in terms of the dimensionless variables, can be written as

$$1 = x^2 + y^2 + z^2 - 2ux. \quad (28)$$

When doing dynamical analysis of this system, it is convenient to use the equation for u too. Taking the derivative of the expression in eq. (17) we find

$$u' = -2\epsilon_H u + 24H^2\xi_{,\phi\phi}x. \quad (29)$$

	x_c	y_c	u_c	z_c	Expansion rate ϵ_{Hc}	If κ is	$\epsilon_{Hc} u_c$
M	0	0	0	1	$\frac{3}{2}(1+w_m)$	any κ	0
K\pm	± 1	0	0	0	3		
I	$\frac{\lambda}{\sqrt{6}}$	$\sqrt{1 - \frac{\lambda^2}{6}}$	0	0	$\frac{1}{2}\lambda^2$		
Sc	$\sqrt{\frac{3}{2}} \frac{1+w_m}{\lambda}$	$\frac{\sqrt{\frac{3}{2}}(1-w_m^2)}{\lambda}$	0	$\sqrt{1 - \frac{3(1+w_m)}{\lambda^2}}$	$\frac{3}{2}(1+w_m)$		
dS	0	1	$-\sqrt{\frac{3}{2}}\lambda$	0	0		
S2	$\sqrt{\frac{3}{2}} \frac{1+w_m}{\kappa}$	0	$\sqrt{\frac{3}{2}} \frac{3(w_m^2-1)}{\kappa(3w_m+1)}$	$\sqrt{1 + \frac{3(3w_m-7)(1+w_m)^2}{2\kappa^2(3w_m+1)}}$	$\frac{3}{2}(1+w_m)$	$\kappa \neq \lambda$	$\neq 0$
G	β	0	$\frac{\beta^2-1}{2\beta}$	0	$\frac{5\beta^2+1}{\beta^2+1} = \sqrt{\frac{3}{2}}\kappa\beta$		
S3	$\sqrt{\frac{3}{2}} \frac{1+w_m}{\lambda}$	$\frac{\sqrt{\frac{3}{2}}(1-w_m^2) + \frac{\lambda}{\sqrt{6}}(1+3w_m)u_c}{\lambda}$	u_c	$\sqrt{1 - \frac{3(1+w_m) - \frac{\lambda}{\sqrt{6}}(5+3w_m)u_c}{\lambda^2}}$	$\frac{3}{2}(1+w_m)$	$\kappa = \lambda$	
IV	x_c	$\sqrt{1 - x_c^2 + 2x_c \cdot \frac{3x_c - \sqrt{\frac{3}{2}}\lambda}{1 + \sqrt{\frac{3}{2}}\lambda x_c}}$	$\frac{3x_c - \sqrt{\frac{3}{2}}\lambda}{1 + \sqrt{\frac{3}{2}}\lambda x_c}$	0	$\sqrt{\frac{3}{2}}\lambda x_c$		

Table I. The values of x , y , u and z parameters at the fixed points and curves. The conditions for the existence of these fixed points and curves can be derived from the fact that all x_c , y_c , u_c and z_c values must be real. Parameters λ , κ and β are defined in eqs. (23), (30) and (A10) respectively. Both λ and κ are strictly positive.

A few comments about these equations are in order. First, notice that taking $u = 0$ ($\xi = \text{const}$) we recover the same equations as used for models in General Relativity (e.g. ref. [35]). In those models, the dimensionless variables y and z are constrained within the range $[0; 1]$ and $x \in [-1; 1]$. This can be seen from eq. (28) or equivalently from eq. (22). In the case of the GB models such restrictions do not apply. As mentioned above, *a priori* the sign of u (or Ω_{GB}) is not determined. Hence, the maximum values of $|x|$, y and z are not limited to 1. Second, eq. (27) diverges as $ux \rightarrow -1$. However, this value is never reached because it falls within the phase space region that is forbidden by the constraint equation (28).

IV. THE EXPONENTIAL GAUSS-BONNET COUPLING

A. Dynamics

To understand the qualitative behaviour of this dynamical system, we find its fixed points and investigate their stability. The fixed points are defined as points, or regions, in the phase space where $x' = y' = z' = 0$ is satisfied. First, we study the case of the exponential GB function, given by

$$\xi = \xi_0 e^{\kappa\phi/m_{\text{Pl}}}, \quad (30)$$

which allows us to write eq. (29) as

$$u' = \left(\sqrt{6}\kappa x - 2\epsilon_H \right) u. \quad (31)$$

The computation details for finding fixed points are provided in the **Appendix** and the results are summarised in Table I.

Looking at this table, notice that all the fixed points with $u_c = 0$ coincide with the ones analysed in ref. [35], as expected. In this reference the authors analyse a quintessence model within the theory of GR and the exponential scalar field potential. In other words, all the fixed points that are present in a similar setup in GR, they are also present in GB models. However, even if the fixed points coincide, the presence of the GB term might change their stability, as we will show below.

The fixed point **M** in Table I corresponds to the case where the scalar field is diluted and only the matter field remains. The **K \pm** fixed points correspond to kination, where the universe is dominated by the kinetic energy of the

scalar field. In the case of **I** and $\lambda < \sqrt{2}$ this fixed point represents the power law inflation [36]. In the scaling fixed point (**Sc**) the evolution of the scalar field adjusts to mimic the behaviour of the matter field. Therefore, the expansion rate of the Universe is given by $\epsilon_H = \frac{3}{2}(1 + w_m)$.

The GB term introduces two more scaling solutions: the fixed point **S2**, which exists for $\kappa \neq \lambda$, and the fixed curve **S3**, which exists if $\xi(\phi)V(\phi) = \text{constant}$. For our purpose, the most interesting new fixed point is the de Sitter one (**dS**), where $\dot{H} = 0$. This fixed point is very robust, and exists for large variety of $\xi(\phi)$ functions.

Some discussion of DE models with $\kappa = \lambda$ and various solutions were provided in Ref. [16]. Some dynamical analysis with $\kappa \neq \lambda$ was performed in Ref. [18] (see also [37]). Here we modify and extend the analysis to make it more generic. In this section, we take $\kappa \neq \lambda$.

Often, the stability of fixed points can be determined by taking a linear perturbation of equations (24)–(29) around those points. In the case of an exponential GB function in eq. (30) those linear equations can be written as

$$\delta x' = (\epsilon_{Hc} - 3)\delta x + \sqrt{6}\lambda y_c \delta y + (1 - \epsilon_{Hc})\delta u + (x_c - u_c)\delta \epsilon_H, \quad (32)$$

$$\delta y' = -\sqrt{\frac{3}{2}}\lambda y_c \delta x + \left(\epsilon_{Hc} - \sqrt{\frac{3}{2}}\lambda x_c\right)\delta y + y_c \delta \epsilon_H, \quad (33)$$

$$\delta u' = \sqrt{6}\kappa u_c \delta x + \left(\sqrt{6}\kappa x_c - 2\epsilon_{Hc}\right)\delta u - 2u_c \delta \epsilon_H, \quad (34)$$

$$\delta z' = \left[\epsilon_{Hc} - \frac{3}{2}(1 + w_m)\right]\delta z + z_c \delta \epsilon_H, \quad (35)$$

where

$$\delta \epsilon_H = \frac{u_c \delta x' + x_c \delta u' + [6x_c - (\epsilon_{Hc} + 1)u_c]\delta x - x_c(1 + \epsilon_{Hc})\delta u + 2\epsilon_{Hc}z_c \delta z}{1 + u_c x_c} \quad (36)$$

is the linearised eq. (27). The constraint equation fixes the dynamics onto the three-dimensional hypersurface in the four-dimensional phase space. The linearised version of that equation is given by

$$0 = (x_c - u_c)\delta x + y_c \delta y + z_c \delta z - x_c \delta u. \quad (37)$$

We next compute the eigenvalues of the system of equations (32)–(35) and determine their stability. The eigenvalues at the fixed point **M** are

$$m_1 = \epsilon_{Hc} - 3, \quad (38)$$

$$m_2 = \epsilon_{Hc}, \quad (39)$$

$$m_3 = -2\epsilon_{Hc}, \quad (40)$$

where $\epsilon_{Hc} = \frac{3}{2}(1 + w_m)$ is the value of the Hubble flow parameter at **M**. We can see that this fixed point is always a saddle point for the range of w_m values that we consider.

The eigenvalues at the kination fixed points (**K \pm**) are

$$m_1 = \frac{3}{2}(1 - w_m), \quad (41)$$

$$m_2 = -6 \pm \sqrt{6}\kappa, \quad (42)$$

$$m_3 = 3 \mp \sqrt{\frac{3}{2}}\lambda, \quad (43)$$

where the upper sign corresponds to the point **K+**. We can see that the eigenvalue m_1 , which corresponds to the eigenvector $\mathbf{v} = (0, 0, 0, 1)^3$, is always positive. Hence, these two fixed points are never stable.

The eigenvalues at the scaling fixed point **Sc** are

$$m_1 = 2\left(\frac{\kappa}{\lambda} - 1\right)\epsilon_{Hc}, \quad (44)$$

$$m_{\pm} = -\frac{1}{2}(3 - \epsilon_{Hc})\left[1 \pm \sqrt{1 - \frac{8\epsilon_{Hc}}{3 - \epsilon_{Hc}} \cdot \left(1 - 2\frac{\epsilon_{Hc}}{\lambda^2}\right)}\right]. \quad (45)$$

³ We order eigenvector components as $\mathbf{v} = (v_x, v_y, v_u, v_z)$.

As can be seen from Table I, this fixed point exists ($z_c^2 \geq 0$) only if $\lambda^2 > 2\epsilon_{Hc}$. Such a condition makes the real part of m_\pm always negative. Therefore the stability of this fixed point is determined solely by the sign of m_1 . That is, the scaling fixed point **Sc** is a saddle point for $\kappa > \lambda$.

The eigenvalues at the de Sitter fixed point **dS** are

$$m_1 = -\frac{3}{2}(1+w_m), \quad (46)$$

$$m_\pm = -\frac{3}{2} \left[1 \pm \sqrt{1 + \frac{8\lambda^2}{3(2+3\lambda^2)} \left(1 - \frac{\kappa}{\lambda} \right)} \right]. \quad (47)$$

Notice that the condition for the stability of this fixed point is exactly opposite from the one required by the scaling fixed point **Sc**: for $\kappa > \lambda$ the scaling fixed point is a saddle and the de Sitter one is the attractor. That is, only one point is attractive, either **dS** or **Sc**, depending on the magnitude of κ/λ ratio. None of the interesting solutions pass through the fixed points **G** or **S2** so we don't analyse their stability here.

To visualise the behaviour of the system we integrate numerically a set of trajectories and show the phase portraits in Figure 1. All the trajectories in the plots start from $y_0 = 10^{-3}$ and move towards the **dS** attractor at $y = 1$. We start our simulations with a negligible GB contribution, $u_0 = -10^{-25}$ to be precise. A few examples of phase portraits with other values of u_0 are shown in Appendix B. Positive u_0 values are not viable for our purpose to explain DE. All such trajectories move towards large values of $u > 0$, away from the de Sitter fixed point **dS** (see Figure 5). Another option is to take negative values of u_0 and $|u_0| \sim \mathcal{O}(1)$. As we can see in Figure 5, this option could provide promising candidate trajectories to explain Dark Energy. This is due to the fact that a large portion of phase space initially evolves towards $u \rightarrow 0$, reaches the scaling fixed point **Sc** and then follows the same evolution pattern as the trajectories with $|u_0| \ll 1$. Nevertheless for our analysis we choose $|u_0| \ll 1$, as this increases the parameter space for viable candidate trajectories. Such small values are also consistent with the scenario proposed in ref. [20], where the GB contribution is negligible initially.

The physically interesting trajectories are those that start close to the **K±** or **M** fixed points. The former set corresponds to the kination initial conditions and the latter ones corresponds to a universe where matter dominates initially. In both cases most trajectories are first attracted to the scaling fixed point **Sc**. But because this fixed point is a saddle point for $\kappa/\lambda > 1$, eventually all the trajectories are repelled and move to the de Sitter attractor **dS**.

This represents the desirable sequence of events: initially the universe is dominated by the kinetic energy of the scalar field, which is the case for quintessential inflation models, or the matter component, which is often encountered in the quintessence models. Next, the system moves into the scaling fixed point, and for a long time the Universe evolves with an effective equation of state that of the matter component.

In the case of GR models and the exponential potential $V(\phi)$, the scaling fixed point **Sc** is an attractor [35]. That is, all the trajectories converge onto this point and remain there. This is problematic, because the universe is not accelerating at **Sc** in contrast to observations. The GB term, on the other hand, converts this point into a saddle one and provides an escape route. The scalar field eventually can come to dominate and cause the universe to expand in an accelerated fashion in a new de Sitter attractor point **dS**.

In Figure 2 we show the time evolution of the density parameters and the effective equation of state of the “dark fluid”. The density parameters are defined in eqs. (19)-(21). As discussed below eq. (22), these parameters are not bounded to lie at or bellow 1, which can be also seen in the bottom right plot.

In order to apply the observational bounds on the equation of state of Dark Energy we define a new parameter w_f . It can be interpreted as the equation of state of an effective “dark fluid” that causes the accelerated expansion. To do that eq. (14) can be written as

$$\epsilon_H = \frac{3}{2} \frac{\rho_\phi(1+w_f) + \rho_m(1+w_m)}{\rho_\phi + \rho_m}, \quad (48)$$

where

$$w_f \equiv \frac{P_\phi + 8H^2(\ddot{\xi} - \dot{\xi}H)}{\rho_\phi} \quad (49)$$

and ρ_ϕ and P_ϕ are the energy and pressure densities of the scalar field defined in eqs. (11) and (12). In terms of dimensionless variables in eq. (17) the last expression can be also written as

$$w_f = -1 + \frac{\frac{2}{3}\epsilon_H(1+2ux) - z^2(1+w_m)}{x^2+y^2}, \quad (50)$$

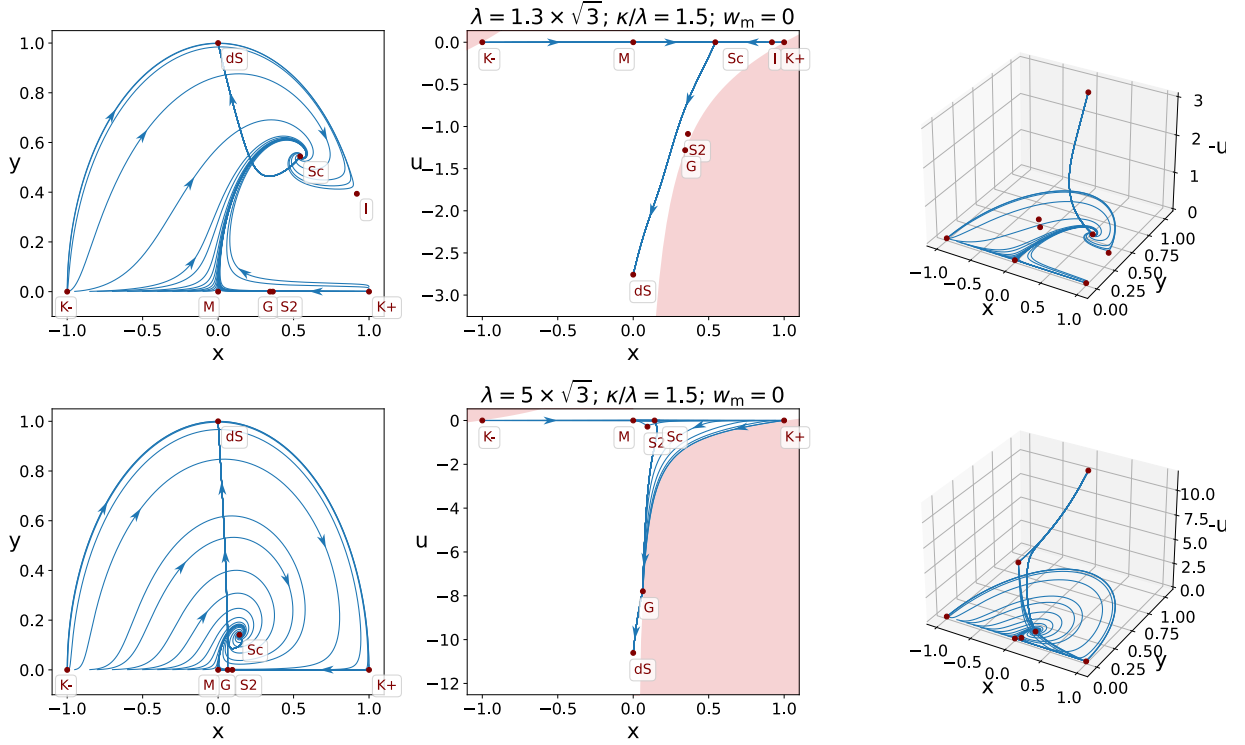


Figure 1. The phase portrait of the dynamical system given by eqs. (24), (25) and (31), with the matter component represented by a pressureless fluid, $w_m = 0$. All trajectories start with very small values of y and u . The first two columns show a projection of the 3 dimensional phase space. The full 3D portrait is displayed in the last column. Red regions in the second column mark forbidden regions of the phase space, where the constraint equation (28) cannot be satisfied for all values of y and z . For those values the constraint in eq. (28) cannot be satisfied. The upper plot corresponds to $\lambda = 1.3 \times \sqrt{3}$ and the lower one to $\lambda = 5\sqrt{3}$. In both cases $\kappa/\lambda = 3/2$.

where ϵ_H is meant to be substituted with eq. (27).

We next run a large number of numerical simulations of eqs. (24), (25) and (31) varying λ , κ parameters as well as the initial conditions x_0 (but always with $u_0 = -10^{-25}$ and $w_m = 0$) and select those models which have regions where $\Omega_m = 0.3147 \pm 0.0074$ and $w_f = -0.957 \pm 0.08$ [21] are satisfied for the same value of N . The scale factor is normalised such that $a = 1$ ($N = 0$) at that moment.

In Figure 2 we show two of such models. On the L.H.S. column we can see the phase portraits, where these models (red curves) are drawn from and on the R.H.S. column we find the time evolution of the density parameters and w_f . Both models have an initial period of kination, which quickly gives way to the matter domination. The model in the upper plot, has a long period of the scaling behaviour before GB energy takes over. Eventually, all the models settle down at the de Sitter attractor point, where $\Omega_\phi = 1$ and all other Ω 's vanish.

In the lower panel of Figure 2 we can also notice a quite generic feature of GB Dark Energy models, namely, that for a brief period of time the effective equation of state of the dark fluid can drop below -1 .

B. The Speed of Gravitational Waves

Obviously, to select a realistic model of DE the consistency with observational constraints on Ω_m and w_f parameters is a necessary but not sufficient condition. There are some other requirements that a viable model of cosmology must satisfy. Among those requirements, especially in the case of GB model, is a negligibly small deviation of the speed of gravitational waves c_{GW} from the speed of light.

As it was pointed out in [5], generically in scalar-GB models $c_{GW} \neq 1$. Due to the tight observational constraints on c_{GW} (see eq. (1)) it was deemed that GBDE models are excluded. However, such constraints do not fix $c_{GW} = 1$, they only place upper bounds on the deviation from 1, albeit very strong ones. And, as one could naively conclude from eq. (8), that bound is not very constraining for GB models of DE. Moreover, in GB models, c_{GW} is not a constant,

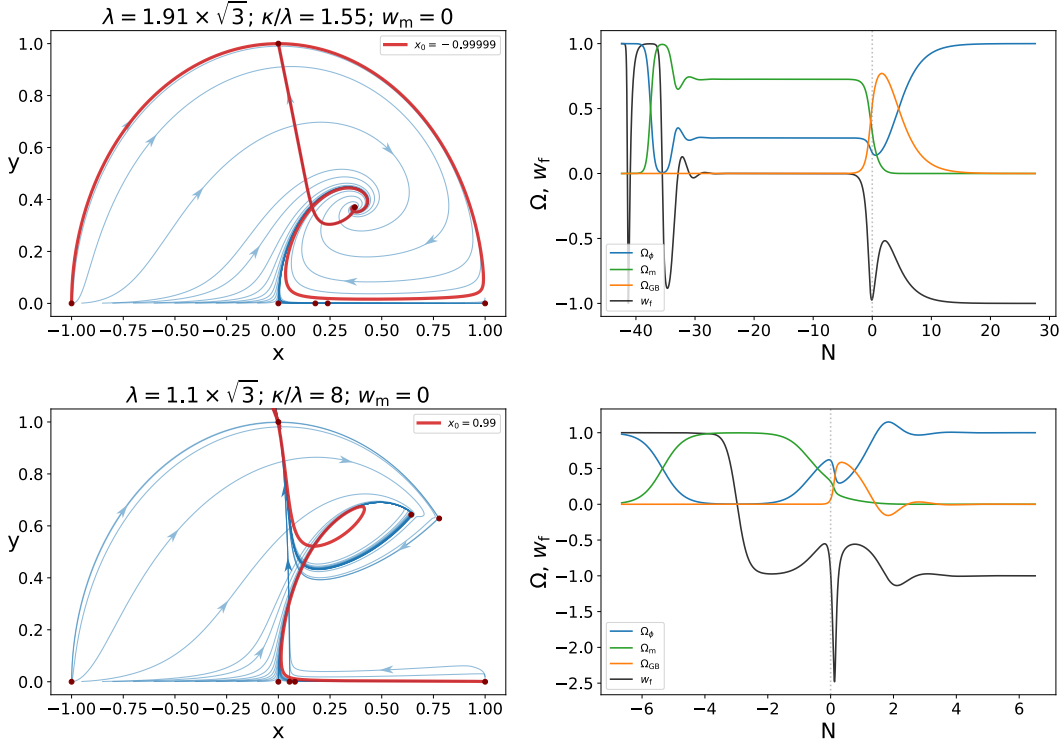


Figure 2. The time evolution of the density and the effective equation of state for two selected trajectories (denoted by red curves on the left column). They are selected such that Ω_m and w_f are consistent with present day observations.

but varies with time. But the constraint in eq. (1) applies only for a short period over the history of the Universe.

To investigate this issue let us first write eq. (5) in terms of dimensionless variables, defined in eq. (17)

$$\alpha_T = \frac{(ux)' + (\epsilon_H - 1)ux}{ux + 1/2} = \frac{\Omega'_{\text{GB}} + (\epsilon_H - 1)\Omega_{\text{GB}}}{\Omega_{\text{GB}} - 1}, \quad (51)$$

where Ω_{GB} is defined in eq. (21). It might appear that α_T diverges at $ux = -1/2$, or equivalently at $\Omega_{\text{GB}} = 1$. But, as can be seen from the constraint equation (28), such a value is not allowed.

We can immediately notice from eq. (51) that α_T vanishes at the two fixed points, **Sc** and **dS**. These fixed points are the most interesting ones. Unfortunately, if the GB model is to be a good model of our Universe, the current stage of the evolution cannot be represented by any of these two fixed points. Instead, we should find ourselves somewhere on the trajectory between **Sc** and **dS**, as it is also demonstrated in Figure 2.

To see how α_T evolves with time we ran a large number of simulations with λ and κ values in the range $1/\sqrt{3} \leq \lambda \leq 20\sqrt{3}$ and $1.1 \leq \kappa/\lambda \leq 20$. In all of these simulations we took $w_m = 0$ and the initial values $y_0 = 10^{-3}$, $u_0 = -10^{-25}$ and a range of x_0 values. Among all the trajectories we selected the ones that satisfy the above discussed bounds on Ω_m and w_f . Some of those solutions are shown in Figure 3. For clarity we depict only a few of them. However, the ones displayed in Figure 3 are representative of the whole set. In particular, we always observe that the maximum value of α_T is very close to $N = 0$, exactly where the observational bounds in eq. (1) apply. In the figure this bound is denoted by the red rectangle, which resembles a vertical line due to its narrowness. The width of this rectangle corresponds to $\Delta N \simeq 0.0098$ [38]. As can be seen in the inset of this figure, the maximum value of $|\alpha_T|$ today is always $\mathcal{O}(0.1) - \mathcal{O}(1)$, which clearly falls outside the allowed range. Hence, with high confidence we can conclude that GBDE models with an exponential coupling constant $\xi(\phi)$ are excluded by the observational constraint on the speed of gravitational waves.

To get some insight why α_T is so large at this particular moment, we can write eq. (51) in an alternative form

$$\alpha_T = 2(\epsilon_H - 3) + 3(1 - w_m) \frac{\Omega_m}{1 - \Omega_{\text{GB}}} + 6 \frac{y^2}{1 - \Omega_{\text{GB}}}. \quad (52)$$

This equality can be obtained either by using the dynamical equations (24)–(29) to eliminate the time derivative from eq. (51), or directly from eq. (14). In any case, it is important to notice that this expression is very generic: it is

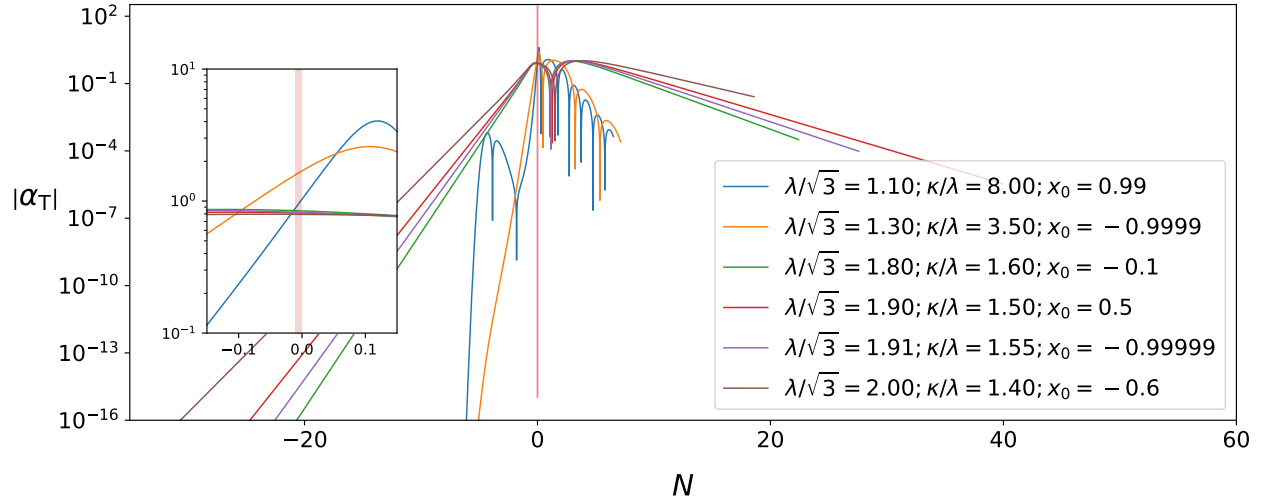


Figure 3. The deviation of the speed of gravitational waves from the speed of light (see eq. (2)) as a function of time. $N = 0$ represents the moment where the model predicts Ω_m and w_f values consistent with present day observations. This is also the moment where the bound in eq. (1) applies (denoted by the very narrow vertical red rectangle). Obviously all models violate this bound by many orders of magnitude. The inset zooms in the region where the curves cross the forbidden values.

valid for any potential $V(\phi)$ and any GB coupling $\xi(\phi)$, not necessarily exponential. At $N = 0$ observations require $\epsilon_H \sim 0.5$. Hence, the absolute value of the first term is of order ~ 1 . Observations also require $w_m = 0$ and $\Omega_m \sim 0.3$. We can use the latter in the constraint in eq. (22) to write $\Omega_\phi + \Omega_{\text{GB}} \sim 0.7$. Moreover, between the scaling fixed point **Sc** and the de Sitter one **dS**, the GB density parameter $\Omega_{\text{GB}} > 0$. Therefore, $0 < \Omega_{\text{GB}} < 0.7$ and the second term in eq. (52) must be of order $\mathcal{O}(0.1)$ to $\mathcal{O}(1)$. Finally $y^2 \leq \Omega_\phi < 0.7$ and the last term of order $\mathcal{O}(1)$ at the maximum. Barring precise cancellations, this leads to the conclusion that generically $|\alpha_T| \sim \mathcal{O}(0.1) - \mathcal{O}(1)$.⁴

V. THE LINEAR GAUSS-BONNET COUPLING

As we have seen above, models with an exponential GB coupling could potentially provide a reasonable history of the Universe and explain DE. Unfortunately, such models predict the speed of GW in the current Universe that violates the allowed values by many orders of magnitude. In this section we investigate another option: the linear GB coupling

$$\xi \propto \phi. \quad (53)$$

As it is shown in the Appendix, such a dynamical system has the same fixed points as the $\epsilon_{Hc} u_c = 0$ subset in Table I.

To study the stability of those fixed points, we can linearise eqs. (24)–(29) and use $\xi_{,\phi\phi} = 0$. Equivalently, we can use the results in section IV by setting $\kappa = 0$. This gives the eigenvalues at the **Sc** point

$$m_1 = -3(1 + w_m), \quad (54)$$

$$m_{\pm} = -\frac{1}{2}(3 - \epsilon_{Hc}) \left[1 \pm \sqrt{1 - \frac{8\epsilon_{Hc}}{3 - \epsilon_{Hc}} \cdot \left(1 - 2\frac{\epsilon_{Hc}}{\lambda^2} \right)} \right]. \quad (55)$$

As discussed in section IV the real part of m_{\pm} eigenvalues are always negative. We can also see from the first equation above that m_1 is negative too. Hence, this fixed point is always an attractor.

On the other hand, the eigenvalues at the de Sitter fixed point **dS** are

$$m_1 = -\frac{3}{2}(1 + w_m), \quad (56)$$

⁴ The observation that $\Omega_m \sim 0.1$ quite generically leads to $|\alpha_T| \gtrsim 0.1$ raises another question. As it follows from eq. (8), such a large value of $|\alpha_T|$ implies a very large change in the GB coupling. But one has to remember that the GB term is only the lowest order term in the series of low-energy effective string theory corrections [9, 12, 13]. Since ξ varies so much, one must wonder if it is consistent to neglect the higher order corrections over the whole range of the evolution.

$$m_{\pm} = -\frac{3}{2} \left[1 \pm \sqrt{1 + \frac{8\lambda^2}{3(2+3\lambda^2)}} \right]. \quad (57)$$

It is clear that $m_1, m_+ < 0$ and $m_- > 0$. Hence, this fixed point is a saddle.

What the above result shows is that a realistic cosmological scenario is impossible with the linear GB coupling. The scaling fixed point is an attractor and there are no solutions which display a long matter dominated period followed by an accelerated expansion. This is also demonstrated in Figure 4.

One might wish to generalise the analysis presented here to higher order polynomial or other functions $\xi(\phi)$ as, for example, considered in refs. [39, 40] in the context of astrophysical compact objects. Unfortunately, other functional forms of $\xi(\phi)$ are not amenable to the presented methods of analysis, as the equations become non-self-similar. Therefore, the relevance of other $\xi(\phi)$ functions in explaining Dark Energy is left for future investigations.

VI. THE CASE OF $\alpha_T = 0$

As can be seen from the expression of α_T in eq. (5) this parameter can be made to vanish if one arranges for the GB coupling in such a way that its time evolution obeys the condition in eq. (6). Unfortunately, this condition does not provide us with a functional form of $\xi(\phi)$. Nevertheless, it provides with enough information to investigate the relevant aspects of such a dynamical system.

First, notice that eq. (6), written in terms the dimensionless variables in eq. (17), becomes

$$24H^2\xi_{,\phi\phi}x^2 = u[(\epsilon_H + 1)x - x']. \quad (58)$$

It provides an additional constraint that can be used to eliminate the $\xi_{,\phi\phi}$ term in eq. (A7), at least for fixed points with $x_c \neq 0$. Otherwise the LHS of the above equation vanishes in any case. The fixed points are computed in the Appendix and summarised in Table II. As one would expect, all the fixed points with $u_c\epsilon_{Hc} = 0$ are the same as in Table I.

To determine the stability of fixed points we again linearise eqs. (24)–(29) and also eq. (58). At the de Sitter fixed point **dS** this linear system reduces to

$$\delta x' = \delta x, \quad (59)$$

$$\delta u' = (4 + 3\lambda^2)\delta x, \quad (60)$$

$$\delta z' = -\frac{3}{2}(1 + w_m)\delta z, \quad (61)$$

where we used that the linearised eq. (58) at **dS** implies the constraint $\delta x' = \delta x$. Combined with the linearised eqs. (24) and (28) we find $\delta u = (4 + 3\lambda^2)\delta x$. It is easy to compute the eigenvalues, which are

$$m_1 = 0, \quad (62)$$

$$m_2 = 1, \quad (63)$$

$$m_3 = -\frac{3}{2}(1 + w_m). \quad (64)$$

We can see that the last two eigenvalues have opposite signs. Hence, in this case **dS** is a saddle fixed point, no longer an attractor.

In the neighbourhood of the scaling fixed point **Sc**, the linear equation for δu takes the form

$$\delta u' = (1 - \epsilon_{Hc})\delta u, \quad (65)$$

where $1 - \epsilon_{Hc} = -\frac{1}{2}(1 + 3w_m)$ is always negative within the range $0 \leq w_m < 1$. Therefore, in the u direction of the phase space this fixed point is attractive and there are no trajectories that flow from **Sc** to **dS**.

In summary, the condition $c_{GW} = 1$ implies the scaling fixed point **Sc** to be an attractor, just as in models of GR [35] and **dS** becomes a saddle point. This leads to the conclusion that there are no solutions which reproduce a long, matter-like domination period and asymptotically approach the de Sitter solution, which is required to reproduce the evolution of the Universe.

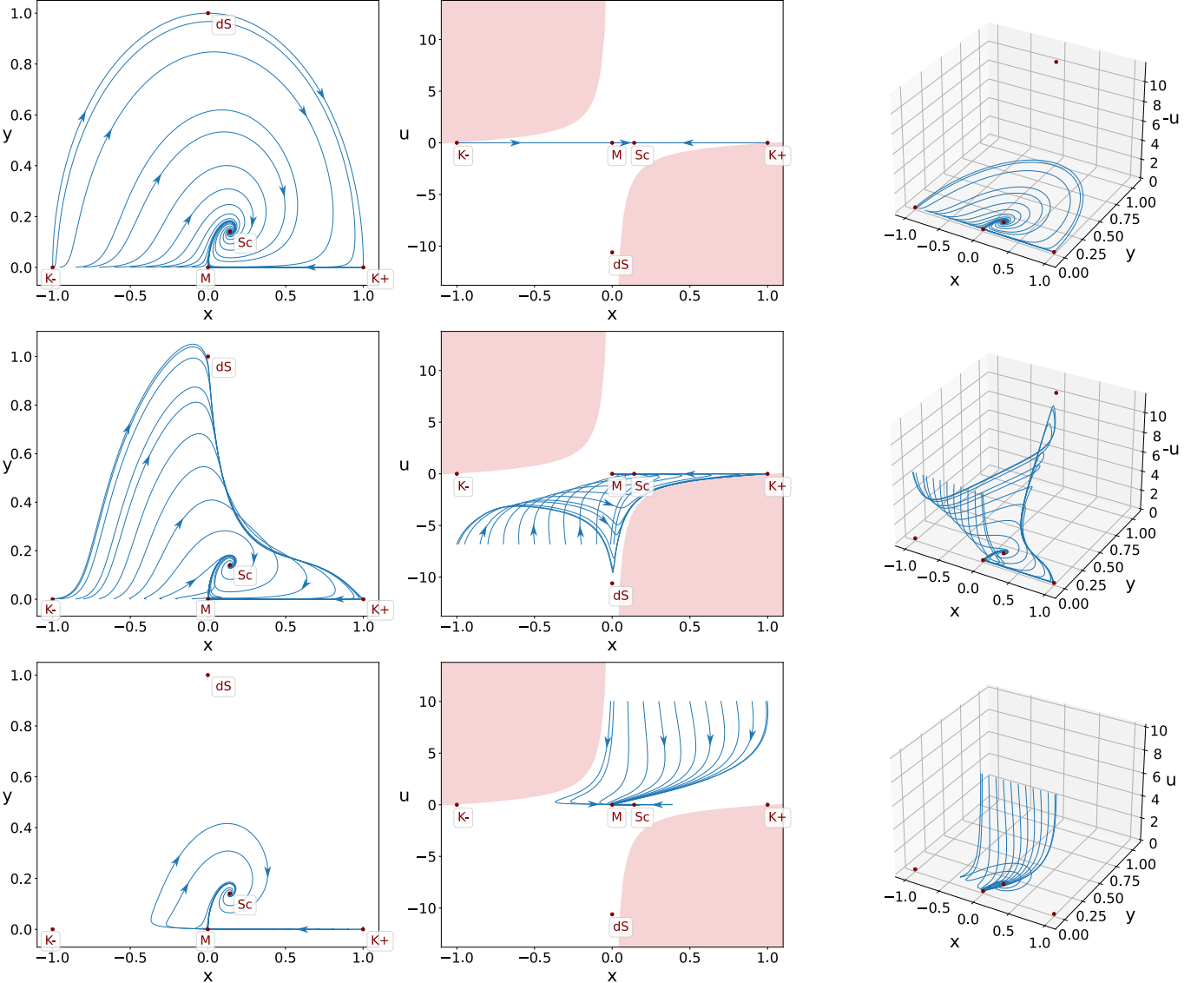


Figure 4. The phase space of the linear model, with $\xi(\phi)$ defined in eq. (53). The notation and the red shaded regions are the same as in Figure 1. All three rows correspond to the same model with $\lambda = 5\sqrt{3}$ and $w_m = 0$, but different initial conditions of u . In the first row $u_0 = -10^{-25}$. As we can see the evolution remains within the $u = 0$ plane. To demonstrate that the scaling fixed point **Sc** is an absolute attractor we also run simulations with large initial values $|u_0|$. In the second row we can see that some trajectories are initially attracted towards the de Sitter fixed point **dS**, but since for a linear $\xi(\phi)$ this point is a saddle, eventually all trajectories converge onto **Sc**. Notice that in the last column we plot $-u$ on the vertical axis of the first two plots and $+u$ of the third plot.

VII. SUMMARY AND CONCLUSIONS

In this work we investigate Gauss-Bonnet Dark Energy (GBDE) models. Generically such models predict the speed of gravitational waves different from the speed of light. In view of the tight observational constraints on such deviations, denoted by α_T (see eq. (1)), such models are considered to be disfavoured. However, the deviation is time dependent and the bound, although tight, is an upper bound, which is only applicable for very late Universe. Hence, before excluding GBDE models we need to perform a more detailed analysis. Moreover, if the bound in eq. (1) is expressed in terms of the variation of the GB coupling function $\xi(\phi)$, it might appear to be a weak bound, as shown in eq. (8).

To see if GBDE models can indeed survive the observational constraints on α_T we perform the dynamical systems analysis. We assume that the scalar field has an exponential potential and find that such a dynamical system quite

	x_c	y_c	u_c	z_c	Expansion rate ϵ_{Hc}
M	0	0	0	1	$\frac{3}{2}(1+w_m)$
K±	± 1	0	0	0	3
I	$\frac{\lambda}{\sqrt{6}}$	$\sqrt{1 - \frac{\lambda^2}{6}}$	0	0	$\frac{1}{2}\lambda^2$
Sc	$\sqrt{\frac{3}{2}} \frac{1+w_m}{\lambda}$	$\frac{\sqrt{\frac{3}{2}}(1-w_m^2)}{\lambda}$	0	$\sqrt{1 - \frac{3(1+w_m)}{\lambda^2}}$	$\frac{3}{2}(1+w_m)$
dS	0	1	$-\sqrt{\frac{3}{2}}\lambda$	0	0
IV	$\sqrt{\frac{2}{3}} \frac{1}{\lambda}$	$\frac{2}{\sqrt{3}\lambda}$	$\sqrt{\frac{3}{2}} \frac{1}{\lambda} \left(1 - \frac{\lambda^2}{2}\right)$	0	1

Table II. Fixed points of the dynamical system that satisfies $\alpha_T = 0$.

generically has the scaling and de Sitter fixed points (among others), denoted by **Sc** and **dS** respectively in this work.

At **Sc** the scalar field adjusts in such a way that it mimics the behaviour of the background matter component. In particular, the equation of state of the scalar field is the same as that of the matter component. In the case of the exponential GB coupling, depending on the magnitude of the exponent, **Sc** is not stable: it is a saddle point. This is in contrast to the General Relativistic quintessence models with an exponential potential [35]. In the latter setup the scaling fixed point is an attractor, which makes it impossible to use as an explanation for the accelerated expansion of the Universe. In GBDE **Sc** can have an unstable direction which links to **dS**, the latter being an attractor. Using numerical solutions we show that if the universe starts with a very small GB term and it is either kination or matter dominated, initially all solutions evolve towards the **Sc** fixed point. They linger in the neighbourhood of **Sc** for a long period of time and eventually change its course towards **dS**. This behaviour is beneficial to modelling quintessential inflation, because it allows, without extreme fine-tuning, to bridge the enormous energy density gap (110 orders of magnitude) between inflation and dark energy. We find numerous models that follow this scenario and can predict observationally allowed values for the matter energy density and DE equation of state.

Moreover, at **Sc** and **dS** fixed points the speed of gravitational waves is exactly the same as that of the speed of light, i.e. $\alpha_T = 0$. Unfortunately, if this model is to represent the evolution of the actual Universe, we cannot be living either on the scaling or de Sitter fixed points, but somewhere in between. However, as we show in Figure 3, $|\alpha_T|$ changes from 0 to ~ 1 in between these fixed points. Moreover, as we argue below eq. (52), if $\Omega_m \sim 0.1$, which corresponds to the current value, quite generically one expects $|\alpha_T| \sim \mathcal{O}(0.1) - \mathcal{O}(1)$, which is ruled out by many orders of magnitude. We conclude that the bound in eq. (1) makes GBDE with an exponential $\xi(\phi)$ function unviable.

In view of the above conclusion, we investigated other choices of $\xi(\phi)$. First, we demonstrate that for a linear function $\xi(\phi)$ the de Sitter fixed point is a saddle point, and the Scaling fixed point becomes an attractor. This makes it impossible to find any viable solution that would be consistent with the evolution of the Universe. We cannot apply our method to study more generic functions $\xi(\phi)$, such as monomials or steeper than exponential potentials studied, for example, in Refs. [39, 40]. This is because dynamical equations lose their self-similar character.

The advantage of the above described analysis is that we have an explicit $\xi(\phi)$ function. But as we showed, this does not provide a viable cosmological solution. Another hope to make GBDE models conform to observational constraints is to impose the condition $\alpha_T = 0$, as can be seen in eq. (5). In this case we lose the benefit of having an explicit functional form of $\xi(\phi)$, but we gain an additional constraint equation (58). As it is demonstrated in Section VI, the stability of fixed points in this case is very similar to the linear model. That is, there are no solutions which provide a long period of matter domination followed by an accelerated expansion.

In summary, we find that a GBDE model with an exponential scalar field potential and an exponential GB coupling function could provide a realistic model of DE. However, the recent bounds on the speed of GW rules out this possibility by many orders of magnitude. If, on the other hand, we look for models that do satisfy $\alpha_T = 0$, then it is impossible to find a scenario consistent with other cosmological observations.

The negative conclusions reached in this work apply to the metric formulation of the Gauss-Bonnet model. But we know that some modified gravity models that violates the α_T bound in eq. (1) become viable again in the Palatini formalism [41]. One can hope that a similar modification could save the GBDE model too.⁵ We intend to study this

⁵ Analogously, if the GB term is coming from the breaking of the Weyl symmetry, also a Weyl term should be added to the action (see

possibility in future publications.

ACKNOWLEDGMENTS

M.K. is supported by the María Zambrano grant, provided by the Ministry of Universities from the Next Generation funds of the European Union. This work is also partially supported by the MICINN (Spain) projects PID2019-107394GB-I00/AEI/10.13039/501100011033 (AEI/FEDER, UE). K.D. was supported, in part, by the Lancaster-Manchester-Sheffield Consortium for Fundamental Physics under STFC grant: ST/T001038/1. A.R. is supported by the Estonian Research Council grant PRG1055.

For the purpose of open access, the authors have applied a Creative Commons Attribution (CC BY) license to any Author Accepted Manuscript version arising.

Appendix A: The Fixed Points

In this section we derive fixed points of the dynamical system in eqs. (24)–(28) that are summarised in Table I. Such points, or higher dimension structures, are regions of the phase space where $x' = y' = z' = 0$. We denote the constant values of x , y , z at these regions by x_c , y_c , z_c . *A priori* we do not impose the condition $u' = 0$ at fixed points, but it follows from the equations. In order to see that we can take the derivative of the constraint equation with respect to N . At a fixed point this gives

$$u'|_{x=x_c} x_c = 0. \quad (\text{A1})$$

This equation allows for $u' \neq 0$ if $x_c = 0$. However, if we plug $x' = x_c = 0$ into eq. (24) and (27) we find

$$0 = \sqrt{\frac{3}{2}}\lambda y_c^2 + u(1 - \epsilon_{Hc}), \quad (\text{A2})$$

where, in this case, ϵ_{Hc} is the value of ϵ_H in eq. (27) at $x' = y' = z' = x_c = 0$. As it is clear from the above equation, all quantities on the RHS are constant but u . Hence, $u = u_c$ must be also a constant even for $x_c = 0$. In summary, the algebraic equations to find fixed point values are given by

$$0 = (\epsilon_{Hc} - 3)x_c + \sqrt{\frac{3}{2}}\lambda y_c^2 + u_c(1 - \epsilon_{Hc}), \quad (\text{A3})$$

$$0 = \left(\epsilon_{Hc} - \sqrt{\frac{3}{2}}\lambda x_c\right)y_c, \quad (\text{A4})$$

$$0 = \left[\epsilon_{Hc} - \frac{3}{2}(1 + w_m)\right]z_c, \quad (\text{A5})$$

where

$$\epsilon_{Hc} = \left[3x_c^2 + \frac{3}{2}(1 + w_m)z_c^2 - u_c x_c\right] \frac{1}{1 + u_c x_c} \quad (\text{A6})$$

and all the values have to satisfy the constraint in eq. (28). There are four possible solutions of this system:

A: $(x, y, u) = \left(x_c, 0, \frac{3(w_m-1)}{3w_m+1}x_c\right)$, which is valid for any value of x_c . The expansion rate in this case is given by $\epsilon_{Hc} = \frac{3}{2}(1 + w_m)$. We can see that this is the scaling solution, where the scalar field adjusts to the equation of state of the matter component.

B: $(x, y, u) = \left(x_c, 0, \frac{x_c^2-1}{2x_c}\right)$ with $\epsilon_{Hc} = \frac{5x_c^2+1}{x_c^2+1}$

C: $(x, y, u) = \left(x_c, \sqrt{1 - x_c^2 + 2x_c \frac{3x_c - \sqrt{\frac{3}{2}}\lambda}{1 + \sqrt{\frac{3}{2}}\lambda x_c}}, \frac{3x_c - \sqrt{\frac{3}{2}}\lambda}{1 + \sqrt{\frac{3}{2}}\lambda x_c}\right)$ with $\epsilon_{Hc} = \sqrt{\frac{3}{2}}\lambda x_c$

for instance Refs. [42, 43]).

D: $(x, y, u) = \left(\sqrt{\frac{3}{2} \frac{1+w_m}{\lambda}}, \sqrt{\frac{\frac{3}{2}(1-w_m^2) + \frac{\lambda}{\sqrt{6}}(1+3w_m)u_c}{\lambda}}, u_c \right)$ with $\epsilon_{Hc} = \frac{3}{2}(1+w_m)$. This is a second scaling solution, which is valid for any (allowed by the constraint) value of u_c .

As we can see, these “fixed points” are actually curves in the three dimensional phase space. In the case of **A** to **C**, the curves are parametrised by the x_c value, which can vary within the range where y , u and z remain real. In the case of **D**, the value of x is fixed to $x_c = \sqrt{\frac{3}{2} \frac{1+w_m}{\lambda}}$, but u is free to vary within the similarly defined range.

We can infer more about the structure of fixed points if we use the definition u in eq. (17). Taking the derivative of that expression we get eq. (29), which we rewrite it here for convenience:

$$u' = -2\epsilon_{Hc}u + 24H^2\xi_{,\phi\phi}x. \quad (\text{A7})$$

Hence, at fixed points we get the relation

$$12H^2\xi_{,\phi\phi}x_c = \epsilon_{Hc}u_c. \quad (\text{A8})$$

If we take an exponential GB function, given in eq. (30), the above equation becomes

$$\sqrt{\frac{3}{2}}\kappa x_c u_c = \epsilon_{Hc}u_c. \quad (\text{A9})$$

Note, that we did not cancel u_c factors, because $u_c = 0$ is an allowed solution. Plugging various values, that are consistent with this equation, into the system **A**–**D**, we obtain fixed points that are summarised in Table I. In that table $x_c = \beta$ at the fixed point **G**. This is a solution of the cubic equation, which is given by

$$\beta \equiv \frac{1}{3\sqrt{3}\kappa} \left(5\sqrt{2} + \frac{9\kappa^2 - 50}{\alpha^{1/3}} - \alpha^{1/3} \right), \quad (\text{A10})$$

where

$$\alpha \equiv \sqrt{2}(27\kappa^2 - 250) + \sqrt{2(27\kappa^2 - 250)^2 + (9\kappa^2 - 50)^3} \quad (\text{A11})$$

and κ is an exponent of $\xi(\phi)$.

It is interesting to note that all fixed points with $u_c\epsilon_{Hc} \neq 0$ (**S2**, **G**, **S3** and **IV**) exist only if the GB function $\xi(\phi)$ is of the form

$$\xi(\phi) = c_1 \frac{\phi}{m_{\text{Pl}}} + c_2 e^{\kappa \frac{\phi}{m_{\text{Pl}}}}, \quad (\text{A12})$$

where $c_2 \neq 0$ and $\kappa = \sqrt{2/3} \cdot \epsilon_{Hc}/x_c$. Or, more precisely, it is sufficient that the GB function asymptotically approaches this solution, as the trajectory in the phase space gets closer to those fixed points. This result can be obtained by integrating eq. (A8) and using the fact that for $x_c\epsilon_{Hc} \neq 0$ we have

$$H = H_0 e^{-\frac{\epsilon_{Hc}}{\sqrt{6}x_c} \frac{\phi}{m_{\text{Pl}}}}. \quad (\text{A13})$$

For the linear $\xi(\phi)$, i.e. for $\xi_{,\phi\phi} = 0$, it follows from eq. (A8) that only fixed points with $\epsilon_{Hc}u_c = 0$ are present. Their values are summarised in Table I.

In the case of $\alpha_T = 0$ constraint, eq. (58) at a fixed point can be written as

$$24H^2\xi_{,\phi\phi}|_c x_c^2 = (\epsilon_{Hc} + 1)x_c u_c. \quad (\text{A14})$$

For fixed points with $x_c = 0$ this equation vanishes identically. Looking at the system **A**–**D**, we see that only two such fixed points exist: $(x, y, u) = (0, 0, 0)$ and $(x, y, u) = \left(0, 1, -\sqrt{\frac{3}{2}}\lambda\right)$. These correspond to points **M** and **dS** in Table I. For $x_c \neq 0$ we can equate eq. (A8) with (A14) and get

$$2\epsilon_{Hc}u_c = (\epsilon_{Hc} + 1)u_c. \quad (\text{A15})$$

For $u_c = 0$ the equation vanishes identically and we obtain the same fixed points as $u_c = 0$ points in Table I. On the other hand, there is only one fixed point that satisfies $u_c \neq 0$. That fixed point must have $\epsilon_{Hc} = 1$. Looking at the system **A**–**D**, we can see that only one such point is allowed, which is the relation **C** with $(x, y, u) = \left(\sqrt{\frac{2}{3}}\frac{1}{\lambda}, \frac{2}{\sqrt{3}\lambda}, \sqrt{\frac{3}{2}}\frac{1}{\lambda}\left(1 - \frac{\lambda^2}{2}\right)\right)$. All these fixed points are summarised in Table II.

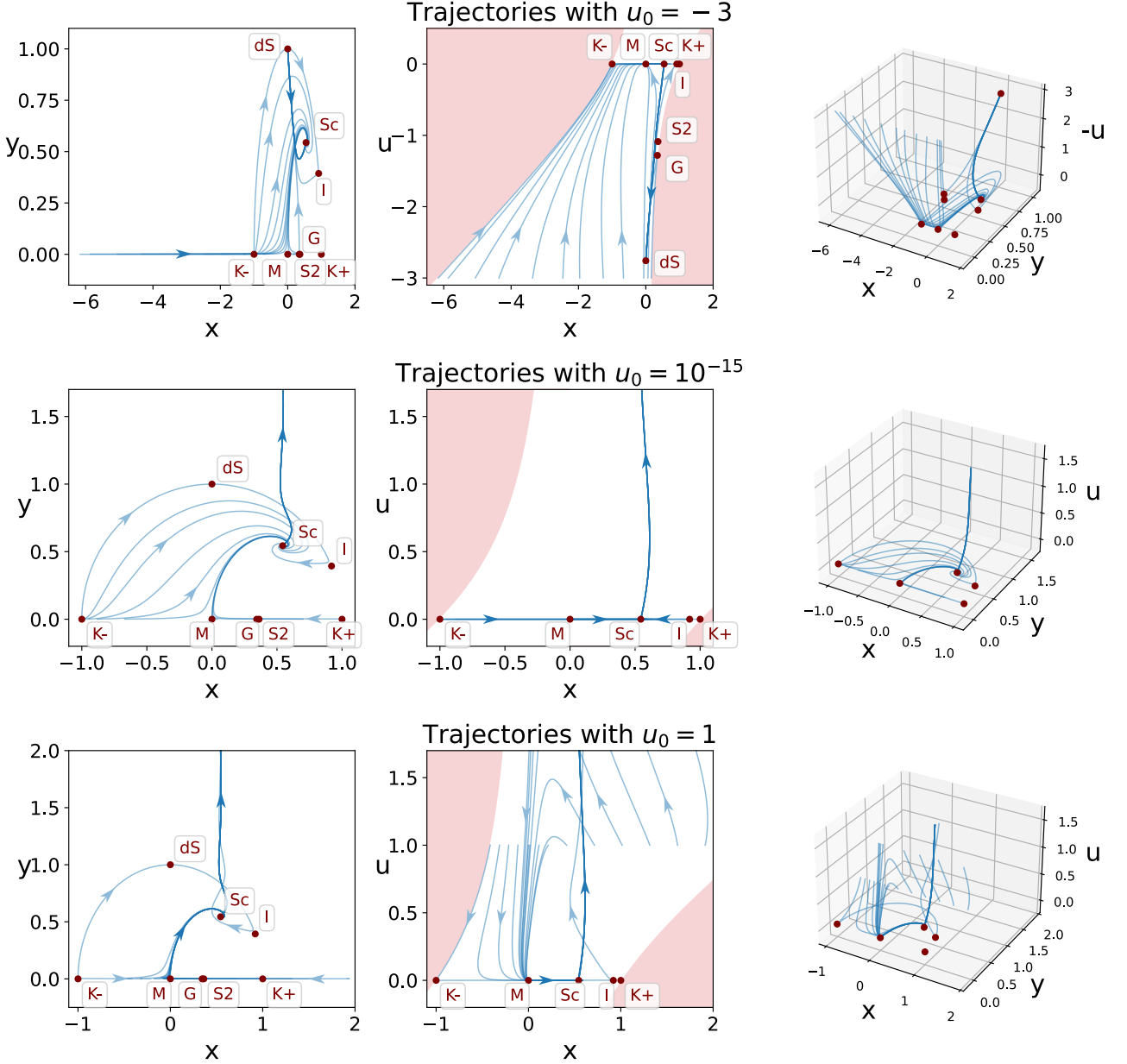


Figure 5. A few examples of phase portraits with different initial values u_0 . The notation, including the red shaded regions, is the same as in Figure 1. All models correspond to the same value $\lambda = 1.3 \times \sqrt{3}$, $\kappa/\lambda = 3/2$ and $w_m = 0$. These values are also used in the upper row of Fig. 1. Notice that the vertical axis of the upper right column is $-u$.

Appendix B: Phase Portraits with More Generic Initial Values

In Fig. 1 we show the phase portrait for the exponential GB coupling with two sets of values of λ and κ . All displayed trajectories start with the initial value $u_0 = -10^{-25}$ in that figure. The absolute value of u_0 is chosen to make the GB term completely negligible initially. This choice is partly motivated by simplicity, because, as can be seen in Fig. 5, the dynamics between the scaling fixed point Sc and the de Sitter one dS is not affected much, at least for some part of the trajectories. Small initial u_0 values are also motivated by the model in ref. [20], where the GB term does not affect the early dynamics of the universe. The sign of u_0 , on the other hand, is crucially important: only those trajectories that satisfy $u_0 < 0$ can eventually be attracted towards dS fixed point. We find that the sign of u is preserved by the evolution equations.

To demonstrate all these points, we provide several plots in Fig. 5 with numerically integrated trajectories for

several u_0 values. For clarity we display plots with negative and positive initial u values separately. Also note that we choose the value of κ that is close to λ . If the ratio κ/λ is too large, the attraction towards the **Sc** fixed point becomes weak, and most of the trajectories do not pass close to this point. This observation is valid for positive as well as negative u_0 initial conditions.

-
- [1] B. P. Abbott *et al.* (LIGO Scientific, Virgo), Phys. Rev. Lett. **116**, 061102 (2016), arXiv:1602.03837 [gr-qc].
[2] B. P. Abbott *et al.* (LIGO Scientific, Virgo), Phys. Rev. Lett. **116**, 241103 (2016), arXiv:1606.04855 [gr-qc].
[3] B. P. Abbott *et al.* (LIGO Scientific, Virgo), Phys. Rev. Lett. **119**, 161101 (2017), arXiv:1710.05832 [gr-qc].
[4] B. P. Abbott *et al.* (LIGO Scientific, Virgo, Fermi-GBM, INTEGRAL), Astrophys. J. Lett. **848**, L13 (2017), arXiv:1710.05834 [astro-ph.HE].
[5] J. M. Ezquiaga and M. Zumalacárcarregui, Phys. Rev. Lett. **119**, 251304 (2017), arXiv:1710.05901 [astro-ph.CO].
[6] L. Amendola, I. Sawicki, M. Kunz, and I. D. Saltas, JCAP **08**, 030 (2018), arXiv:1712.08623 [astro-ph.CO].
[7] C. G. Callan, Jr., S. R. Coleman, J. Wess, and B. Zumino, Phys. Rev. **177**, 2247 (1969).
[8] D. J. Gross and J. H. Sloan, Nucl. Phys. B **291**, 41 (1987).
[9] D. G. Boulware and S. Deser, Phys. Rev. Lett. **55**, 2656 (1985).
[10] I. Antoniadis, E. Gava, and K. S. Narain, Nucl. Phys. B **383**, 93 (1992), arXiv:hep-th/9204030.
[11] I. Antoniadis, J. Rizos, and K. Tamvakis, Nucl. Phys. B **415**, 497 (1994), arXiv:hep-th/9305025.
[12] M. C. Bento and O. Bertolami, Phys. Lett. B **368**, 198 (1996), arXiv:gr-qc/9503057.
[13] M. Sami, A. Toporensky, P. V. Tretjakov, and S. Tsujikawa, Phys. Lett. B **619**, 193 (2005), arXiv:hep-th/0504154.
[14] R. Aros, M. Contreras, R. Olea, R. Troncoso, and J. Zanelli, Phys. Rev. Lett. **84**, 1647 (2000), arXiv:gr-qc/9909015.
[15] R. Olea, JHEP **06**, 023 (2005), arXiv:hep-th/0504233.
[16] S. Nojiri, S. D. Odintsov, and M. Sasaki, Phys. Rev. D **71**, 123509 (2005), arXiv:hep-th/0504052.
[17] L. Amendola, C. Charmousis, and S. C. Davis, JCAP **12**, 020 (2006), arXiv:hep-th/0506137.
[18] T. Koivisto and D. F. Mota, Phys. Rev. D **75**, 023518 (2007), arXiv:hep-th/0609155.
[19] T. Koivisto and D. F. Mota, Phys. Lett. B **644**, 104 (2007), arXiv:astro-ph/0606078.
[20] C. van de Bruck, K. Dimopoulos, C. Longden, and C. Owen, (2017), arXiv:1707.06839 [astro-ph.CO].
[21] N. Aghanim *et al.* (Planck), Astron. Astrophys. **641**, A6 (2020), [Erratum: Astron. Astrophys. 652, C4 (2021)], arXiv:1807.06209 [astro-ph.CO].
[22] J. M. Cline, S. Jeon, and G. D. Moore, Phys. Rev. D **70**, 043543 (2004), arXiv:hep-ph/0311312.
[23] C. de Rham and S. Melville, Phys. Rev. Lett. **121**, 221101 (2018), arXiv:1806.09417 [hep-th].
[24] H. Noh and J.-c. Hwang, Phys. Lett. B **515**, 231 (2001), arXiv:astro-ph/0107069.
[25] J.-c. Hwang and H. Noh, Phys. Rev. D **71**, 063536 (2005), arXiv:gr-qc/0412126.
[26] J.-c. Hwang and H. Noh, Phys. Rev. D **66**, 084009 (2002), arXiv:hep-th/0206100.
[27] S. D. Odintsov and V. K. Oikonomou, Phys. Lett. B **797**, 134874 (2019), arXiv:1908.07555 [gr-qc].
[28] S. Kawai, M.-a. Sakagami, and J. Soda, Phys. Lett. B **437**, 284 (1998), arXiv:gr-qc/9802033.
[29] S. Kawai and J. Soda, Phys. Lett. B **460**, 41 (1999), arXiv:gr-qc/9903017.
[30] V. K. Oikonomou, Astropart. Phys. **141**, 102718 (2022), arXiv:2204.06304 [gr-qc].
[31] Y. Akrami *et al.* (Planck), Astron. Astrophys. **641**, A10 (2020), arXiv:1807.06211 [astro-ph.CO].
[32] M. Heydari-Fard, H. Razmi, and M. Yousefi, Int. J. Mod. Phys. D **26**, 1750008 (2016).
[33] B. Ratra and P. J. E. Peebles, Phys. Rev. D **37**, 3406 (1988).
[34] C. Wetterich, Nucl. Phys. B **302**, 668 (1988), arXiv:1711.03844 [hep-th].
[35] E. J. Copeland, A. R. Liddle, and D. Wands, Phys. Rev. D **57**, 4686 (1998), arXiv:gr-qc/9711068 [gr-qc].
[36] F. Lucchin and S. Matarrese, Phys. Rev. D **32**, 1316 (1985).
[37] S. Tsujikawa and M. Sami, JCAP **01**, 006 (2007), arXiv:hep-th/0608178.
[38] J. Hjorth, A. J. Levan, N. R. Tanvir, J. D. Lyman, R. Wojtak, S. L. Schröder, I. Mandel, C. Gall, and S. H. Bruun, Astrophys. J. Lett. **848**, L31 (2017), arXiv:1710.05856 [astro-ph.GA].
[39] H. O. Silva, J. Sakstein, L. Gualtieri, T. P. Sotiriou, and E. Berti, Phys. Rev. Lett. **120**, 131104 (2018), arXiv:1711.02080 [gr-qc].
[40] D. Doneva and S. S. Yazadjiev, JCAP **04**, 011 (2018), arXiv:1712.03715 [gr-qc].
[41] M. Kubota, K.-Y. Oda, K. Shimada, and M. Yamaguchi, JCAP **03**, 006 (2021), arXiv:2010.07867 [hep-th].
[42] C. Corianò, M. M. Maglio, and D. Theofilopoulos, Eur. Phys. J. C **82**, 1121 (2022), arXiv:2203.04213 [hep-th].
[43] P. G. S. Fernandes, P. Carrilho, T. Clifton, and D. J. Mulryne, Class. Quant. Grav. **39**, 063001 (2022), arXiv:2202.13908 [gr-qc].